Journal of Power Sources 196 (2011) 4826–4831

Contents lists available at ScienceDirect

Journal of Power Sources

journal homepage: www.elsevier.com/locate/jpowsour

Equivalent circuit model parameters of a high-power Li-ion battery: Thermal and state of charge effects

Jamie Gomez [a], Ruben Nelson [b], Egwu E. Kalu [a,*], Mark H. Weatherspoon [b], Jim P. Zheng [b]

[a] Department of Chemical & Biomedical Engineering, FAMU-FSU College of Engineering, United States
[b] Department of Electrical & Computer Engineering, FAMU-FSU College of Engineering, United States

ARTICLE INFO

Article history:
Received 22 November 2010
Received in revised form
20 December 2010
Accepted 21 December 2010
Available online 15 January 2011

Keywords:
Lithium-ion batteries
Equivalent circuit modeling
SOC
Temperature
Impedance

ABSTRACT

Equivalent circuit model (EMC) of a high-power Li-ion battery that accounts for both temperature and state of charge (SOC) effects known to influence battery performance is presented. Electrochemical impedance measurements of a commercial high power Li-ion battery obtained in the temperature range 20 to 50 °C at various SOC values was used to develop a simple EMC which was used in combination with a non-linear least squares fitting procedure that used thirteen parameters for the analysis of the Li-ion cell. The experimental results show that the solution and charge transfer resistances decreased with increase in cell operating temperature and decreasing SOC. On the other hand, the Warburg admittance increased with increasing temperature and decreasing SOC. The developed model correlations that are capable of being used in process control algorithms are presented for the observed impedance behavior with respect to temperature and SOC effects. The predicted model parameters for the impedance elements R_s, R_{ct} and Y_{013} show low variance of 5% when compared to the experimental data and therefore indicates a good statistical agreement of correlation model to the actual experimental values.

© 2011 Elsevier B.V. All rights reserved.

1. Introduction

In recent times, rechargeable lithium batteries (RLB) remain the top choice for consumer electronics, telecommunication, hybrid power sources as well as other applications due to their high energy density, design flexibility and cost. Predicting battery performance can enhance the convenience, reliability, utility, and mobility of RLBs [1]. Conventionally, equivalent circuits are used to interpret data obtained from electrochemical impedance spectroscopic (EIS) measurements [1]. Conversely, in the ECM approach, the associated equivalent circuit can be used as the tool to predict battery behavior [1]. A previous work in [2] details a schematic of an ECM that contains parameters that are important in the analysis of Li-ion batteries. With the knowledge of the internal workings of a battery, one can predict the discharge power performance, transient and dynamic behavior of Li-ion batteries thus suggesting the use of such models as control algorithms and energy storage designs [2]. However, the exclusion of temperature and SOC effects, known to influence battery performance, leaves a knowledge gap generated in previous works in [2,3] on those parameters analyzed. Thus, there is a need for an analysis that accounts for the influence of both temperature and SOC on the ECM proposed in [2]. Such data can lead to the development of an improved control algorithm for battery systems. The objective of this paper is to apply the technique of ECM in the analysis of the effect of temperature and SOC on the ECM parameters of high power Li-ion battery. Such result for a high power Li-ion battery is not available in the open literature. The behavior of impedance elements present in an ECM under variable thermal and SOC conditions, such as solution resistance, charge transfer resistance, and Warburg impedance are considered.

2. Materials and methods

The battery used in this experiment was a Sony commercial Li-ion polymer battery (UP393562) which has a nominal capacity of 800 mAh. Electrochemical impedance system (EIS) measurements were carried out using Gamry Potentiostat/Galvanostat Reference 3000 machine. Various SOC values between 0% and 100% were obtained with the Arbin BT2000 Battery test system. The operating voltage of a typical Li-ion cell is in the 3.0–4.2 V range. As a result, the cell was charged at a constant current of 0.6 A until the voltage reached 4.2 V. Following this, a constant voltage charge maintained the voltage at 4.2 V until the current decayed to 100 mA. Finally, a constant current discharge at 600 mA led the battery to approach the desired SOC until fully discharged at 3.0 V. The temperature range from 20 to 50 °C was achieved using a temperature controlled chamber. For each new temperature, the battery was allowed to equilibrate for 24 h before conducting charge/discharge cycles and

* Corresponding author. Tel.: +1 850 410 6327; fax: +1 850 410 6151.
E-mail address: ekalu@eng.fsu.edu (E.E. Kalu).

0378-7753/$ – see front matter © 2011 Elsevier B.V. All rights reserved.
doi:10.1016/j.jpowsour.2010.12.107

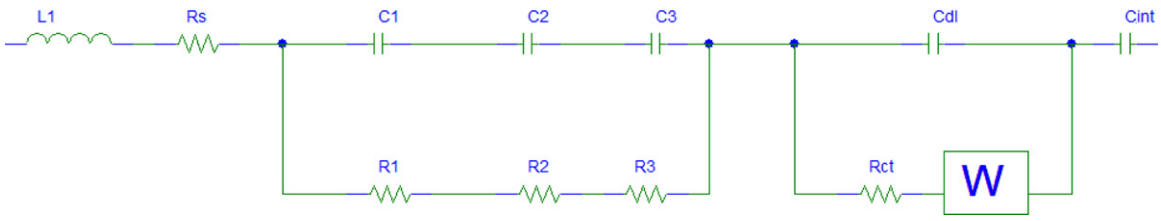

Fig. 1. A simple proposed model circuit for high-power Li-ion battery (L_1 is the inductor, the Warbug impedance W is characterized by admittance, Y_{013} and a time constant, B_{14}).

impedance measurements. The generated plots were limited to a frequency sweep from 20 kHz to 0.01 Hz.

Gamry Echem Analyst software enabled the collection of the data and the construction of the ECM using the graphical model editor. No pre-built models in Echem Analyst were used in the development of the high-power Li-ion battery model.

3. Results and discussion

The data collected showed distinct variation with temperature of key impedances within the Li-ion cell. A simple ECM, as proposed in Fig. 1, identifies the various impedances of this high power Li-ion battery. It utilizes an inductor (L_1) to incorporate the inductive behavior due to electrical energy storage and the geometry of the electrodes, a modified Randles circuit which contains a resistance in series called the solution resistance (R_s), which illustrates the ohmic resistance of the battery; R-C circuits (R_n and C_n) in parallel which denote the slow migration of Li-ions through surface films of the electrode; a charge transfer resistance (R_{ct}) and a double layer capacitance (C_{dl}) of electrodes; diffusion impedance of the anode and cathode also known as Warburg impedance, characterized by admittance (Y_{013}) and a time constant (B_{14}), and finally intercalation capacitance (C_{int}) which describes the accumulation and depletion of Li ions within the electrode [2,4]. It should be noted that the intercalation capacitance was included in this model to show the variation of open circuit potential with SOC [2].

Table 1 shows the values of these ECM parameters at a chosen temperature and SOC along with their confidence intervals. It is noted that parameters such as Y_{013} which are strongly dependent on SOC and temperature fall within their confidence interval.

Fig. 2 shows typical (both experimental and modeled) Nyquist impedance spectra at different temperatures and SOC, where the independent axis is the real impedance (Z') and the dependent axis is the imaginary impedance (Z''). At all temperatures and SOC values, the impedance spectra is comprised of an inductive tail at high frequencies, which is attributed to the porosity of the electrode jelly-roll structure and connection leads to the battery; the high frequency intercept on the real axis represents the total ohmic resistance of the cell, which includes the electrolyte and contact resistance, electronic contacts, etc; depressed semicircles at middle to high frequencies of the spectra can be ascribed to the solid electrolyte interface layer of the electrodes while the semicircle in the mid-frequency range is characteristic of the charge transfer at the electrode/electrolyte interface. The low frequency portion represents the solid-state Warburg diffusion of lithium ions into the porous electrode matrix; extremely low frequencies signify the differential intercalation capacitance of the electrode, which describes the accumulation of lithium ions within the host material [2].

At each SOC it is observed that the charge transfer process depicted by the semicircle becomes more depressed as temperature increases. Also as SOC increases the semicircle increases in both the x and y directions. It is interesting to note that the solid-state Warburg diffusion tail becomes increasingly visible as temperature increases from 30 to 50 °C and as SOC increases from 0 to 100%. This can be explained by an increased diffusion rate at higher temperatures.

Table 1 illustrates predicted values of ECM parameters that show distinct changes with temperature and SOC. At high temperatures, there is a clear decrease in solution and charge transfer resistances relative to their values at the lower temperatures. Under these same

Table 1
Predicted ECM parameter values for R_s, R_{ct} and Y_{013} and Z_{eq} at various temperatures and SOC.

Temperature (°C)	SOC (%)	$R_{ct,pred} \pm 0.02$	$R_{s,pred} \pm 0.0002$	$Y_{013,pred} \pm 0.01$	$Z_{eq,pred} \pm 0.002$
20	0	0.275	0.0858	45.6	0.1404
	10	0.331	0.0868	43.9	0.1435
	50	0.438	0.0898	33.7	0.1489
	80	0.529	0.0908	22.5	0.1492
	100	0.665	0.0908	13.2	0.1493
30	0	0.131	0.0836	54.2	0.1169
	10	0.182	0.0846	52.5	0.1200
	50	0.252	0.0875	42.3	0.1255
	80	0.299	0.0885	31.1	0.1257
	100	0.400	0.0886	21.8	0.1258
40	0	0.047	0.081	75.6	0.1006
	10	0.093	0.0821	73.9	0.1037
	50	0.131	0.0850	63.7	0.1091
	80	0.140	0.0860	52.5	0.1094
	100	0.206	0.0881	43.2	0.1095
50	0	0.029	0.0781	88.0	0.0921
	10	0.072	0.0791	86.3	0.0951
	50	0.084	0.0821	76.1	0.1006
	80	0.056	0.0831	64.9	0.1009
	100	0.091	0.0832	55.6	0.1010

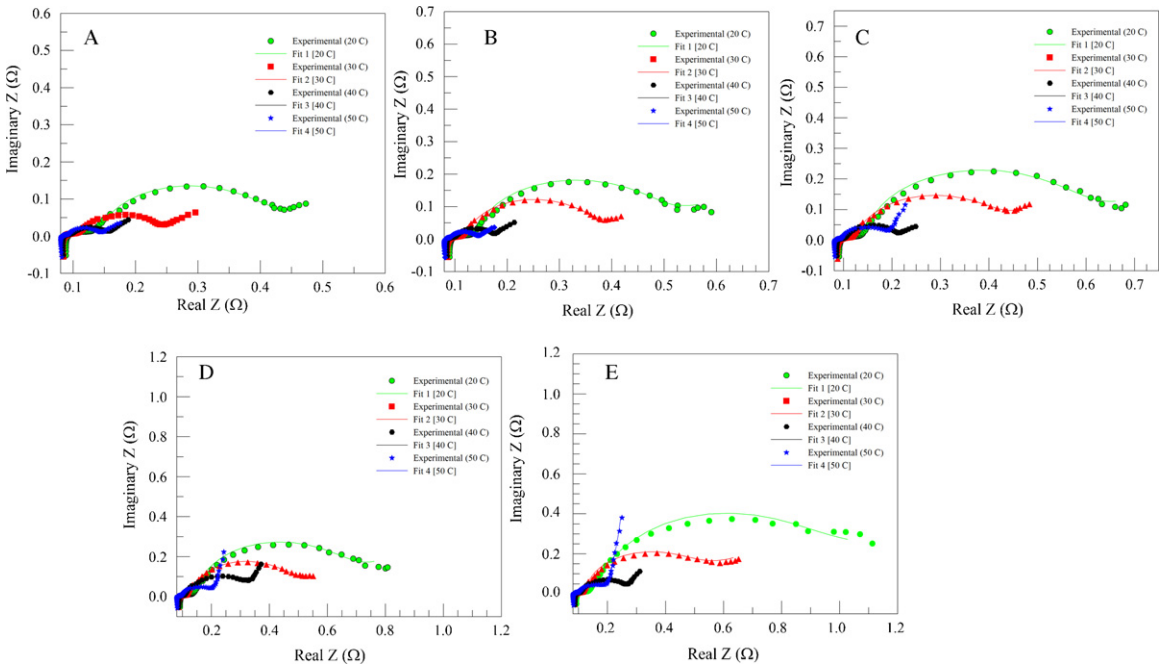

Fig. 2. Nyquist impedance spectra of high-power Li-ion battery at various SOC and different temperatures: (A) 0% SOC, (B) 10% SOC, (C) 50% SOC, (D) 80% SOC, and (E) 100% SOC.

conditions there is an increase in Warburg admittance with increasing temperature. These observed phenomena are discussed later in the paper. Additionally, a *t*-test confirms some parameters such as C_1 and R_3 are not statistically significant. The critical *t* values ($p = 0.002$, $p = 0.001$) for 38 degrees of freedom are 2.712 and 3.319. The calculated *t* value of 2.74 is less than the above values and gives a probability of less than 5%.

The effect of temperature and SOC are further illustrated in Figs. 3–5. The data showed that charge transfer (Fig. 3) and solution (Fig. 4) resistances decreased with increasing temperature and decreasing SOC whilst Warburg admittance (Fig. 5) increased with increasing temperature and decreasing SOC (Table 2).

It is well known that electrons enter the electrode and lithium ions diffuse into the electrolyte thus allowing charge to be transferred. Experimental results depicted in Fig. 3 show that as temperature increases, the charge transfer resistance (R_{ct}) decreases. R_{ct} is related to the reaction kinetics from Butler–Volmer equation for a charge-transfer controlled electrochemical reaction

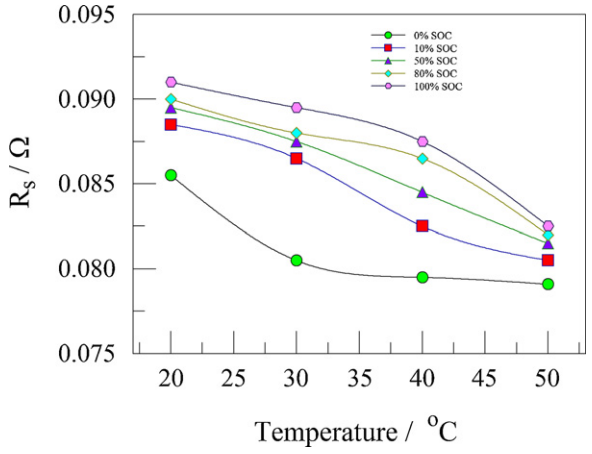

Fig. 4. Effect of temperature on electrolyte resistance of high-power Li-ion battery at various SOC.

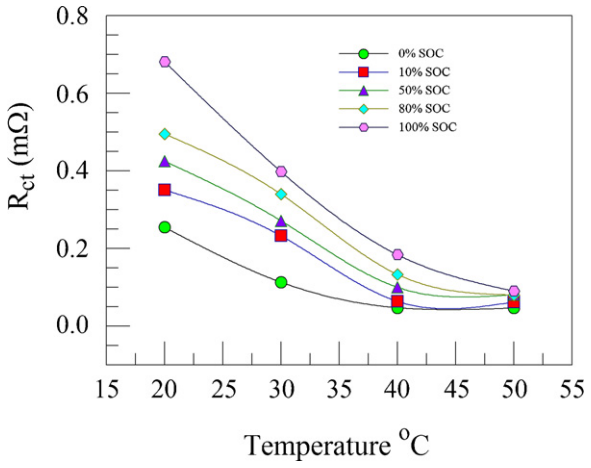

Fig. 3. Effect of temperature on charge transfer resistance of high-power Li-ion battery at various SOC.

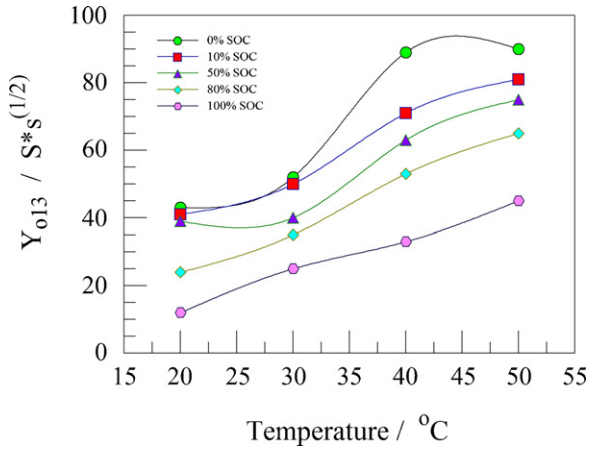

Fig. 5. Effect of temperature on the Warburg impedance of high-power Li-ion battery at various SOC.

Table 2
Model fitting parameters at 50% SOC and 30 °C.

ECM parameter	Value	95% confidence interval	
L_1 (μH)	4.74e^{-7}	4.67e−7	4.82e^{-7}
R_s (mΩ)	8.51e^{-2}	8.37e^{-2}	8.65e^{-2}
R_1 (mΩ)	1.5e^{-2}	8.82e^{-3}	2.58e^{-2}
C_1 (mF)	8.50e^{-3}	−7.57e^{-3}	1.48e^{-1}
R_2 (mΩ)	1.66e^{-2}	−1.13e^{-2}	7.97e^{-2}
C_2 (mF)	1.10e^{-1}	1.04e^{-1}	1.82e^{-1}
R_3 (mΩ)	2.30e^{-3}	2.23e^{-3}	7.48e^{-3}
C_3 (mF)	1.41e^{-2}	9.93e^{-3}	3.32e^{-2}
C_{dl} (F)	2.20	1.62	2.24
R_{ct} (mΩ)	2.52e^{-1}	1.50e−1	3.11e^{-1}
C_{int} (mF)	1.48e^{3}	1.36e^{3}	2.36e^{3}
Y_{013} (S × s$^{1/2}$)	42.3	40.9	61
β_{14} (s$^{1/2}$)	13.7	12.7	16.9

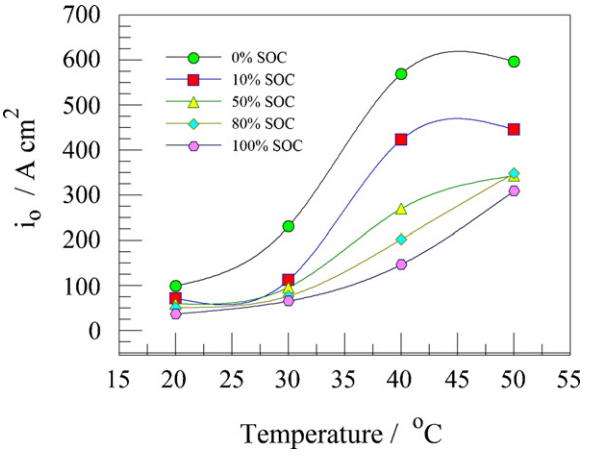

Fig. 6. Variation of exchange current density at various temperatures and SOC values.

[5] by:

$$R_{ct} = \frac{RT}{nFi_o} \tag{1}$$

where R is the gas constant, T is the absolute temperature in Kelvin and i_o is the exchange current density (ECD). The values of i_o were calculated using Eq. (1) at various temperatures and SOC values and shown in Fig. 6. As shown in Fig. 6, at a temperature of 30 °C and below, the ECD values are relatively insensitive to both changes in temperature and SOC values above 0%.

However, above 30 °C, it can be noted that as temperature increases the exchange current density increases hence decreasing R_{ct}. At 0% SOC, the ECD increases with temperature even for temperatures below 30 °C. The variation of ECD with temperature is expected based on the fundamental equation (see Eq. (2)) that depicts i_o as a function of reaction rate coefficient, k – which itself can be expressed as an exponential function of temperature (Arrhenius relationship). However, as SOC decreases towards a fully discharged condition, exchange current increases. The relationship between i_o and concentration (C) of Li ions is given in Eq. (2)

$$i_o = nFk_a^{1-\beta}k_c^{\beta}\prod C_i^{qi+B_{si}} \tag{2}$$

where n is the number of electrons, F is Faraday's number, k_a and k_c are the anodic and cathodic rate constants, respectively and C_i is the concentration of oxidizing and reducing reagents in their standard states, Π is the product and superscript β is the transfer coefficient. SOC may be defined as the ratio of the amount (C_i) of Li that is available for extraction to the maximum (C_s) that can be extracted from the electrode (see Eq. (3)).

$$\text{SOC} = \frac{C_i}{C_s} \tag{3}$$

Consequently we can write

$$C_i = C_s(\text{SOC}) \tag{4}$$

Substituting Eqs. (2) and (4) into Eq. (1) we have

$$R_{ct} = \frac{RT}{FnFnK_a^{1-\beta}k_c^{\beta}\prod[(\text{SOC})C_i]^{q_i+B_{si}}} \tag{5}$$

where q_i and β_{si} represent the coefficients of the cathodic and the anodic reaction, respectively. From the relationship between ECD and R_{ct} shown by Eq. (5) it can be deduced that R_{ct} increases as concentration of Li-ions in the electrolyte increase due to de-intercalation of Li-ions from the cathode. The rate constants (k_a, k_c) which depend on temperature according to Arrhenius law can be written as

$$k_i = A_o e^{-E_a/RT} \tag{6}$$

where subscript i can be anodic or cathodic, A_o is a constant and E_a is the activation energy. Based on the above relationship, it is seen that as temperature increases the exponential term tends to zero which relieves the dependence of the rate constant on temperature. So as concentration of Li-ions increases due to de-intercalation of Li-ions, R_{ct} increases. It can be concluded that k_a and k_c do not contribute to the variation of R_{ct} with temperature.

A trend similar to that observed for charge transfer resistance is noted for the solution resistance which also decreases with increasing temperature, as shown in Fig. 4. At low temperatures, the electrolyte, $LiPF_6$, in ethylene carbonate, leads to high electrolyte viscosity and poor lithium ion transport since the PF_6^- anion is more stable at lower temperatures [6] thus preventing dissociation of the electrolyte and consequently hindering release of the Li^+. It was also found that $LiPF_6$ is not stable at elevated temperatures and decomposes to LiF and PF_5 [7]. An examination of the data of a recent study [8] suggests that the diffusion coefficient of $LiPF_6$ decreases with increasing concentration and decreasing temperature. The increase of ionic conductivity with temperature also contributes to the ease of Li-ion transport through the electrolyte across the separator membrane into the electrode.

The Warburg impedance (Z) is often described by Eq. (7)

$$Z = \sigma(\omega)^{-1/2}(1-j) \tag{7}$$

where the Warburg coefficient is given by Eq. (8)

$$\sigma = \frac{RT}{n^2F^2A\sqrt{2}}\left(\frac{1}{C_o\sqrt{D_o}} + \frac{1}{C_R\sqrt{D_R}}\right) \tag{8}$$

where A is the area of the electrode, C_o and C_R are the concentration of the oxidized and reduced species, respectively. Similarly, D_o and D_R are the diffusion coefficients of the oxidized and reduced species, respectively.

It can be seen that the Warburg coefficient given by Eq. (8) has an inverse relationship with concentration. Therefore as SOC decreases the Warburg coefficient will increase due to reduced active species concentration. The relationship between the Warburg coefficient and Warburg admittance shown by Eq. (9) is a converse trend. The Warburg admittance (Y_{013}) increased with decreasing SOC and increasing temperature as shown in Fig. 5 and it is expected that the Warburg coefficient will decrease with decreasing SOC and increasing temperature. Consequently, from Eq. (7), it can be inferred that the Warburg impedance will decrease with

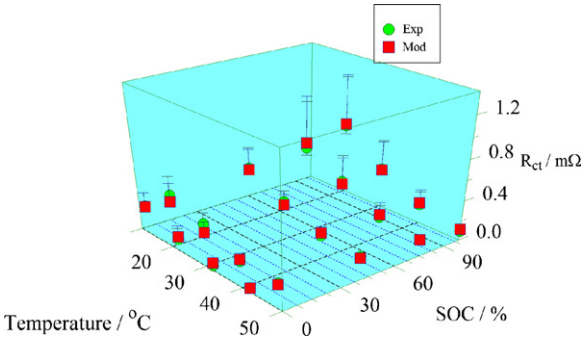

Fig. 7. 3D scatter plot of experimental and model predictions showing the effect of temperature and SOC on charge transfer resistance.

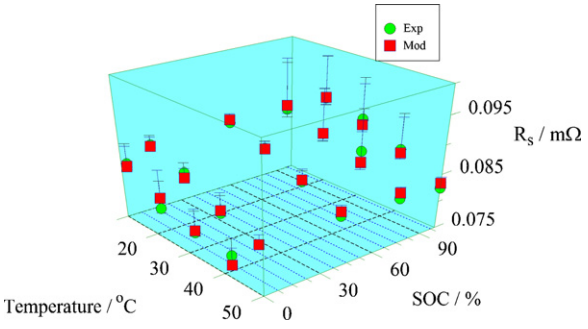

Fig. 8. 3D scatter plot of experimental and model predictions showing the effect of temperature and SOC on solution resistance.

increasing temperature and decreasing SOC.

$$\sigma = \frac{1}{\sqrt{2}Y_{013}} \tag{9}$$

3.1. Model discussion and results

The experimental and modeled 3D scatter plots correlating R_s, R_{ct} and Y_{013} with SOC and temperature are compared and shown in Figs. 7–9, respectively. The positive correlations shown are dictated by electrochemical processes, primarily transfer of Li ions and electrons which induce charge transfer to and from the electrodes, migration of Li-ions through the electrolyte as well as diffusion impedance of the electrodes. Fig. 7 shows an exponential decrease of R_s with increasing temperature and a slow decrease with no sharp drops with SOC as indicated by the scatter plot. There was a 5.1% standard deviation between the predicted and experimental R_s at p-value close to 1.

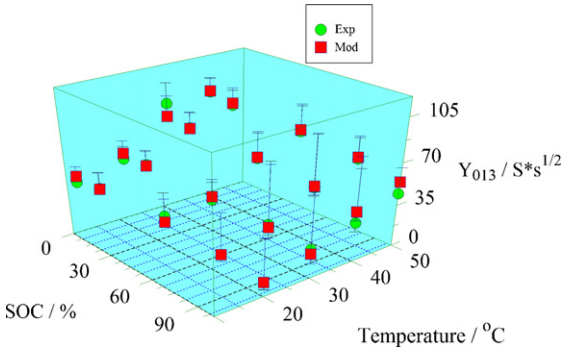

Fig. 9. 3D scatter plot of experimental and model predictions showing the effect of temperature and SOC on Warburg impedance.

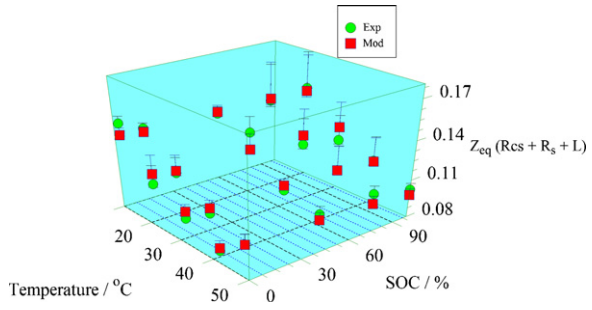

Fig. 10. 3D scatter plot of experimental and model predictions showing the effect of temperature and SOC on combined impedances.

A sharp exponential decrease with increasing temperature is noted in Fig. 8 for R_{ct} at a constant SOC. Results also show that the effect of SOC on R_{ct} is more pronounced at lower temperatures than at higher temperatures. The variance between the experimental and predicted R_{ct} differed by less than 2% with a p-value close to 1 which is indicative of relatively accurate agreement between proposed circuit model and experimental values. A significant temperature and SOC effect on Y_{013} is illustrated in Fig. 9. Y_{013} decreases with increasing SOC and increases exponentially with increasing temperature. The predicted Y_{013} was within 5% variation of the experimental Y_{013} once again showing good agreement. Fig. 10 is a 3D scatter plot representing the combination of L, R_s and RC circuits (see Fig. 1) to give an equivalent impedance $Z_{eq(RCs+Rs+L)}$ and its correlation with SOC and temperature. An exponential decrease with increasing temperature is noted in Fig. 10 for $Z_{eq(RCs+Rs+L)}$ at a constant SOC. There was 5.4% variance between predicted and experimental $Z_{eq(RCs+Rs+L)}$. The following equations (Eqs. (10)–(13)) are provided to account for the influence of temperature and SOC on R_{ct}, R_s and Y_{013} as well as equivalent impedance ($RC_s + R_s + L$) which contributes to the overall equivalent impedance. The experimental temperature and SOC data obtained for R_{ct}, R_s and Y_{013} were used to fit by Levenberg–Marquardt computational algorithm, the empirical equations that optimally describe the dependence of these three parameters on temperature and SOC. Such equations can be utilized in the development of a control algorithm for a high-power Li-ion battery.

$$R_{ct}(R^2 = 0.983) = -6.2e^{-6} + 7.7 \times \mathrm{SOC} + 0.1 \times T - 4.3e^{-2} \times \mathrm{SOC} \times T + 1.1 \times \mathrm{SOC}^2 - 7.1e^{-4} \times T^2 + 1.1e^{-6} \times T^3 + 0.8 \times \mathrm{SOC}^3 + 1.1e^{-6} \times T^3 \tag{10}$$

$$R_s(R^2 = 0.995) = 1.1e^{-6} + 1.1e^{-3} \times \mathrm{SOC} + 7.9e^{-4} \times T - 5.8e^{-3} \times \mathrm{SOC}^2 - 1.7e^{-6} \times T^2 \tag{11}$$

$$Y_{013}(R^2 = 0.963) = -7.5e^{-8} - 15.1 \times \mathrm{SOC} + 346.2 \times T - 17.3 \times \mathrm{SOC}^2 - 3.38 \times T^2 + 1.1e^{-2} \times T^3 - 1.2e^{-5} \times T^4 \tag{12}$$

$$Z_{eq}(R^2 = 0.979) = 5.8e^{-8} + 3.5e^{-2} \times \mathrm{SOC} + 1.6e^{-2} \times T - 4.54e^{-2} \times \mathrm{SOC}^2 - 9.4e^{-5} \times T^2 + 1.9e^{-2} \times \mathrm{SOC}^3 + 1.42e^{-7} \times T^3 \tag{13}$$

where SOC is in its fractional form (e.g. 80% SOC = 0.8), T is the absolute temperature in Kelvin and R^2 gives the coefficient of multiple determination. It should be noted that impedance parameters C_{int}, β_{14}, and C_{dl} appear not to play very critical role within the

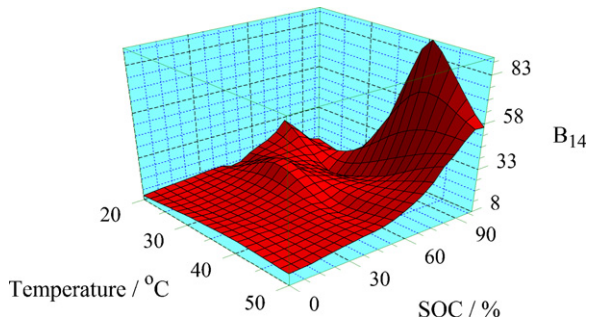

Fig. 11. 3D surface plot of model predicted values of β_{14} showing its variation with temperature and SOC.

scope of these results and no discernible pattern of relationship with temperature and SOC can be inferred at all conditions studied. However for β_{14}, it was observed that within the range of temperatures studied, the β_{14} values initially remain flat as SOC increases up to 30% SOC, then the values rise and decrease again as the 100% SOC is approached. For temperatures above 30 °C, after the above-described relationship with SOC, the values of β_{14} increase exponentially with SOC as the 100% SOC value is approached. The 3D surface plot for the behavior is shown in Fig. 11.

4. Conclusion

The effect of temperature and SOC on a Li-ion polymer battery was investigated. The NLLS fitting procedure consisted of several iterations which produced the best fit equivalent circuit parameters. Overall, the solution resistance and charge transfer resistance decreased as temperature increased and SOC decreased. However, temperature and SOC parameters have the opposite effect on the Warburg admittance, where a higher temperature and lower SOC resulted in increased admittance. Models of combined impedances were created to give the user a plug and chug mechanism to determine the overall impedance given SOC and temperature. The behavior of the individual impedances have been shown to be related to fundamental electrochemical, transport and thermodynamic properties of the battery and this paper provides insight as to the critical role temperature and SOC play on these specific impedances. Based on these results we expect to provide impedance parameter model correlations as functions of temperature and SOC that subsequently can be used to improve battery design and control algorithms.

Acknowledgement

This work was supported by ERC Program of the National Science Foundation under Award Number EEC-08212121.

References

[1] M. Dubarry, B.Y. Liaw, J. Power Sources 174 (2007) 856–860.
[2] P.L. Moss, G. Au, E.J. Plitcha, J.P. Zheng, J. Electrochem. Soc. 155 (12) (2008) A986–A994.
[3] P. Suresh, A.K. Shukla, N. Munichandriah, J. Appl. Electrochem. 32 (2002) 267–273.
[4] F. La Mantia, J. Vetter, P. Novak, Electrochim. Acta (2008) 4109–4121.
[5] A.J. Bard, L.R. Faulkner, Electrochemical Methods, J. Wiley & Sons, New York, 1980, p. 105.
[6] C.L. Campion, W.T. Li, B.L. Lucht, J. Electrochem. Soc. 152 (12) (2005) A2327–A2334.
[7] E. Zinigrad, L. Larush-Asraf, J. Gnanaraj, M. Sprecher, D. Aurbach, Thermochim. Acta 438 (2005) 184–191.
[8] K. Kumaresan, G. Sikha, R.E. White, J. Electrochem. Soc. 155 (2) (2008) A164–A171.